Defect evolution and impurity migration in Na-implanted ZnO

Pekka T. Neuvonen,[1,*] Lasse Vines,[1] Vishnukanthan Venkatachalapathy,[1] Asier Zubiaga,[2] Filip Tuomisto,[2] Anders Hallén,[3] Bengt G. Svensson,[1] and Andrej Yu. Kuznetsov[1]

[1]*Department of Physics, Centre for Material Science and Nanotechnology, University of Oslo, P.O. Box 1048 Blindern, NO-0316 Oslo, Norway*

[2]*Department of Applied Physics, Aalto University, P.O. Box 11100, FI-00076 Aalto, Finland*

[3]*Royal Institute of Technology, School of ICT, Dept. of Microelectronics and Applied Physics, P.O. Box Electrum 229, SE-164 40 Kista, Sweden*

(Received 10 June 2011; revised manuscript received 9 September 2011; published 3 November 2011)

Secondary ion mass spectrometry (SIMS) and positron annihilation spectroscopy (PAS) have been applied to study impurity migration and open volume defect evolution in Na^+ implanted hydrothermally grown ZnO samples. In contrast to most other elements, the presence of Na tends to decrease the concentration of open volume defects upon annealing and for temperatures above 600 °C, Na exhibits trap-limited diffusion correlating with the concentration of Li. A dominating trap for the migrating Na atoms is most likely Li residing on Zn site, but a systematic analysis of the data suggests that zinc vacancies also play an important role in the trapping process.

DOI: 10.1103/PhysRevB.84.205202 PACS number(s): 81.05.Dz, 61.72.uj, 66.30.J−, 61.72.Cc

I. INTRODUCTION

Zinc oxide (ZnO) is a direct wide band-gap (∼3.4 eV) semiconductor with high exciton binding energy (∼60 meV)[1] making it highly desirable for optoelectronic devices, such as light emitting diodes, UV sources/sensors, room-temperature (RT) lasers,[2,3] etc. Recent developments in growth of ZnO[4,5] have made high-quality single crystalline wafers available, giving ZnO an advantage over more traditional direct wide band-gap materials, e.g., nitrides. ZnO wafers exhibit native *n*-type conductivity, although its origin is still under debate. Intrinsic defects, like zinc interstitials (Zn_i) and oxygen vacancies (V_O) have been suggested as responsible for the native *n*-type conductivity,[6–8] whilst other reports state that the formation energy of Zn_i is too high,[9] and the donor level of V_O is too deep[10] to explain the native conductivity. Moreover, different impurities, such as Al, Ga, In, and H are incorporated into ZnO during growth and can act as shallow donors.[11–13] However, none of these impurities alone can account for the donor concentrations observed suggesting contributions from different donorlike defects and impurities.[14]

The major obstacle challenging the realization of bipolar ZnO devices is the unreliable *p*-type doping, which has much in common with those known for other wide band-gap semiconductors:[15,16] (i) acceptor-type dopants exhibit solid solubility below typical native donor concentrations, (ii) acceptors states are deep in the band gap preventing sufficient ionization at RT, or (iii) dopants adopt several configurations in the lattice leading to self-compensation. In particular, atomic configurations of Li and Na in ZnO depend on the position of the Fermi level (E_F); for E_F close to the conduction band edge, Li (Na) atoms on substitutional sites—Li_{Zn} (Na_{Zn})—prevail, while Li (Na) atoms on interstitial sites—Li_i (Na_i)—are favoured when E_F is close to the valence band edge.[17,18] Thus, in *n*-type hydrothermally grown (HT) ZnO, which contains $\gtrsim 10^{17}$ Li/cm^3, the predominant configuration is Li_{Zn}, often resulting in highly resistive material.[19,20]

In this study, the interaction between Li and Na has been investigated by implanting Na into (i) HT samples with a Li content of $\sim 4 \times 10^{17}$ cm^{-3} and (ii) HT samples subjected to postgrowth anneals reducing the Li content to the 10^{15} cm^{-3} range. Especially, secondary ion mass spectrometry (SIMS) and positron annihilation spectroscopy (PAS) have been combined to reveal the role of zinc vacancies (V_{Zn}) in the interaction between Li and Na.

II. EXPERIMENTAL

Four initially high-resistive (*n* type, $\rho \sim 1$ kΩcm) 10×10 mm HT ZnO wafers, labeled A–D and containing $2–4 \times 10^{17}$ Li/cm^3 (called HT Li level), were used. Wafers C and D were heat treated before ion implantation (preannealed) at 1500 °C to reduce the amount of Li by at least two orders of magnitude.[19] Note that the preannealing causes an increase in the Na background concentration from $<10^{15}$ cm^{-3} (wafers A and B) to the 10^{16} cm^{-3} range (wafers C and D) due to furnace contamination. A standard mechanical polishing process using diamond slurry with grain size from 5 μm down to 0.25 μm on rotating nylon suspension disks followed the preanneals of the wafers C and D in order to restore the surface quality. Na implants were performed at RT with an energy of 150 keV resulting in a projected range (R_p) of ∼180 nm. A 7° tilt angle relative to the incident ion beam was used to reduce channeling effects. Wafers A and C were subjected to a dose of 1×10^{14} Na/cm^2 and wafers B and D to 1×10^{15} Na/cm^2. After implantation, the wafers were cut into four pieces labeled as a wafer quarter, e.g., A_1 and A_2, and then annealed in oxygen ambient under different conditions, as summarized in Table I.

Li and Na concentration versus depth profiles were measured by secondary ion mass spectrometry (SIMS) using a Cameca IMS7f microanalyzer. A primary beam of 10 keV O_2^+ ions was rastered over a 125×125 μm^2 surface area and secondary ions were collected from central region of the sputtered crater. Crater depths were measured with a Dektak 8 stylus profilometer, and a constant erosion rate was assumed to convert sputtering time into sample depth. Implanted reference

TABLE I. Processing details and identification of the samples.

Wafer	Pretreatment	Na^+ dose (cm^{-2})	Postanneals 10 min O_2 (°C)
A_1		1×10^{14}	...
A_2		1×10^{14}	600
A_3		1×10^{14}	800
A_4		1×10^{14}	950
B_1		1×10^{15}	...
B_2		1×10^{15}	600
B_3		1×10^{15}	800
B_4		1×10^{15}	950
C_1	X	1×10^{14}	...
C_2	X	1×10^{14}	600
C_3	X	1×10^{14}	800
C_4	X	1×10^{14}	950
D_1	X	1×10^{15}	...
D_2	X	1×10^{15}	600
D_3	X	1×10^{15}	800
D_4	X	1×10^{15}	950

samples were used to quantify the Na and Li signals and for both elements, a detection limit in the low 10^{14} cm^{-3} range was obtained.

Open-volume defect evolution was monitored by positron annihilation spectroscopy (PAS). In PAS, positrons annihilate with electrons in a material and produce 511 keV gamma (γ) radiation. Before the annihilation, positrons can be trapped by neutral or negatively charged open-volume defects or, in some cases, by negative ions. The trapping changes the annihilation characteristics, including Doppler broadening of the γ radiation. This broadening was measured using a Ge detector with an energy resolution of 1.24 keV. The broadened 511-keV-annihilation line is divided into two regions: *S* fraction of annihilations with low momentum electrons ($p_L <$ 0.4 a.u.) and *W* fraction of annihilations with high-momentum electrons (1.6 a.u. $< p_L <$ 4.0 a.u.). Typically, the trapping of positrons at open-volume defects results in narrowing of the annihilation line.[21] The *S* parameter is more sensitive than *W* to changes in open volume of defects, thus in the course of presentation of the results, we emphasize on profiling of *S* parameters as a function of a positron implantation energy. However, the *W* parameter as a function of *S* parameter, i.e., *W*-*S* plots, are also presented. The positrons are introduced (implanted) into the samples in a form of a Makhov profile and the absolute width of the profile increases with increasing implantation energy. Thus, when converting positron energy to depth, the probed region has a considerable width around the mean positron penetration depth. Nominally, the R_p value of ~180 nm corresponds to the mean penetration depth of 7.5 keV positrons. The maximum positron implantation energy used in this study was 36 keV corresponding to a mean penetration depth of ~2.2 μm.

III. RESULTS

A. Li and Na concentration versus depth profiles

Li and Na concentration versus depth profiles for wafers A–D are shown in Figs. 1(a)–1(d), respectively, and they are found to exhibit qualitatively different behavior. Firstly, competition between Na and Li occurs in wafers A and B upon the heat treatment, e.g., Li is depleted from the Na-rich region after 600 °C.[22] Subsequently, Li returns to this region when the Na concentration decreases at higher temperatures.[23]

In the wafer A, Fig. 1(a), a measurable Na diffusion is found at 800 °C (A_3), while the redistribution of Li occurs already at 600 °C (A_2), indicating Li/Na interaction at 600 °C or below.[22] The 800 °C anneal results in a boxlike Na profile with a plateau at ~4×10^{17} cm^{-3} (A_3), characteristic of trap-limited diffusion (TLD), while the sample annealed at 950 °C (A_4) exhibits a long Na tail resembling Fickian diffusion. For the wafer B, Fig. 1(b), the implantation dose is increased by one order of magnitude compared to that for wafer A, and the Na diffusion profiles extend to large depths. In addition, already the 600 °C anneal (B_2) results in a significant redistribution of Na and not of Li only as in wafer A. Furthermore, the Na profiles in wafer B exhibit distinct plateaus around ~2–5 $\times 10^{17}$ Na/cm^3, which increase in width with increasing annealing temperature.

In contrast, wafers C and D do not reveal any significant diffusion of Na into the sample bulk, Figs. 1(c) and 1(d). The Na atoms remain in the implanted region and then display a substantial surface out-diffusion at high temperatures. Further, Li does not show an anticorrelating behavior with Na, as for wafers A and B, but piles up in the implanted region of sample C_2 (as observed also for other implanted elements).[24] However, for sample D_2, Li does not pile up in this same region, most likely because the Li interaction with radiation-induced defects is blocked by higher concentration of Na atoms occupying vacancy-type defects (see Sec. III B). On the other hand, sample D_3, demonstrates a depletion of Li from the mid-10^{15} cm^{-3} to the mid-10^{14} cm^{-3} range beyond the implanted region without any measurable Na diffusion. Interestingly, the 950 °C anneal results in approximately the same Na peak concentration (~8×10^{17} cm^{-3}) for the samples C_4 and D_4, despite one order of magnitude difference in Na dose. This suggests that Na is trapped by defects present in the vicinity of the sample surface but not related to the implantation damage. The polishing procedure used for wafers C and D is known to cause subsurface defects, which progress into the sample during annealing and are stable up to 1100 °C.[25] Hence, the concentration of such defects expected to be identical in the wafers C and D, accounting for the fact that about the same concentration of Na is trapped irrespective of the implantation dose used.

B. Open-volume defect profiles

Figures 2(a)–2(d) display *S* parameters as a function of the positron implantation energy (as well as depth as a top axis) for wafers A–D, respectively, and Fig. 3 represents the corresponding *W*-*S* plots. The data may be readily introduced if we group/discriminate between wafers A/B and C/D, similarly as in Sec. III A. Starting with wafer A, Fig. 2(a), the damage accumulated in the as-implanted sample (A_1) is unveiled in the form of increase in *S* parameter. After annealing at 600 °C (A_2), the further increase of the *S* parameter above the value characteristic of the Zn vacancy, $S = 1.05 \times S_{ZnO\,Ref} =$ 0.439, indicates a formation of large open-volume defects

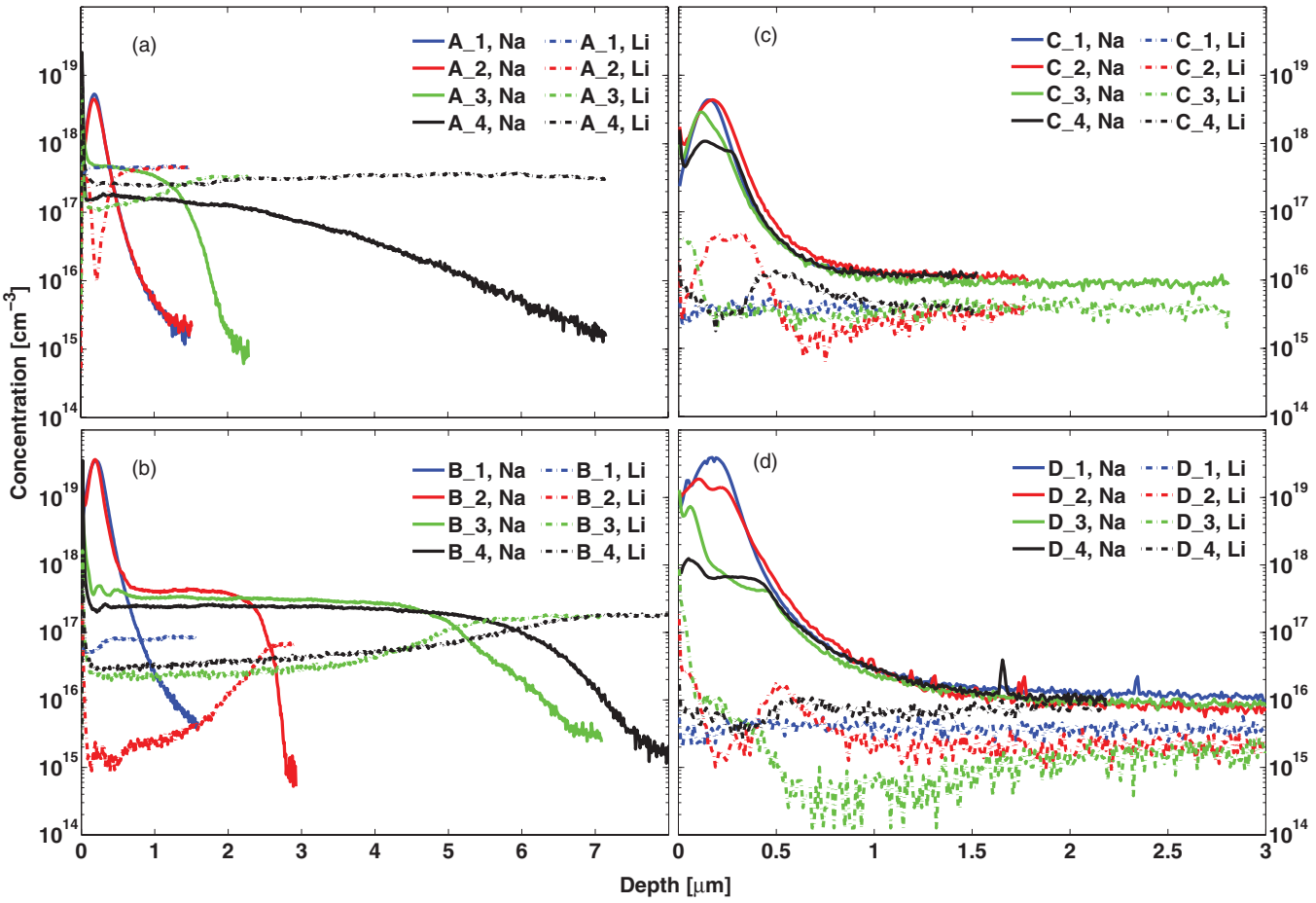

FIG. 1. (Color online) Na (solid) and Li (dot-dash) concentration vs depth profiles for wafers A–D [panels (a)–(d), respectively].

(vacancy clusters), consistent with previous implantation studies.[24,26–30] In terms of depth localization, the clustering occurs between the surface and R_p. Annealing of wafers A and B at temperatures above 600 °C decreases gradually the open-volume defect concentration to values below the PAS detection limit.

More information can be gained from the *W*-*S* plot for wafer A in Fig. 3(a). The parameters are normalized to those of annihilation in the delocalized state in ZnO, labeled as "ZnO bulk" a vapor phase grown ZnO sample (ZnO in Fig. 2), with V_{Zn} concentration below the PAS detection limit, was measured as a reference simultaneously with the studied samples to give the "ZnO-bulk" point. Correspondingly, the "V_{Zn}" point in Fig. 3 is based on positron saturation trapping in V_{Zn}'s as measured in previous experiments.[31–33] If V_{Zn} is the dominating trap for positrons, all data points follow the V_{Zn} line and the position represents the actual V_{Zn} concentration. However, this is not the case in Li-rich samples, where the *W*-*S* data converge below the V_{Zn} line due to positron trapping at Li_{Zn} as shown recently by Johansen *et al.*[20] A similar conclusion can also be drawn from Fig. 3(a) identifying the region just below the ZnO-bulk point, where our data converge ($S \approx 1.005$, $W \approx 0.95$), as the "HT-ZnO" point. It should be noted that the shift in "bulk" *S* and *W* values toward the HT-ZnO point complicates the estimation of the V_{Zn} concentration. However, when the data obey the V_{Zn} line, the V_{Zn} concentration can be deduced using previously obtained values for bulk and defect lifetimes[31] combined with the *S* and *W* parameters obtained in the present study.[34] In its turn, experimental data above the V_{Zn} line combined with high *S* parameter values indicate large (compared with V_{Zn}) open-volume defects, i.e., vacancy clusters where both Zn and O atoms are missing, as clusters of only cation vacancies in compound semiconductors do not produce a deviation from the single vacancy line or its extension.[35] The defects in the as-implanted samples (e.g., A_1) are clearly larger in size than a single V_{Zn}, and after annealing (A_2), they evolve into even bigger vacancy clusters with a size of probably at least 3–5 V_{Zn}'s (and a corresponding amount of V_O's).[36] The results from sample A_3 appear to be closer to the V_{Zn} line than the rest of the data, indicating a smaller contribution from Li_{Zn}, correlating with the Li redistribution in Fig. 1(a). In addition, high-temperature anneals remove a significant part of the implantation-induced defects and the data from sample A_4 converge close to the HT-ZnO point.

The annealing behavior of the B samples, Figs. 2(b) and 3(b), reveals intriguing characteristics to be attributed to the higher Na dose as compared to that for wafer A. In Fig. 2(b), a large reduction of the implantation damage occurs already at 600 °C (B_2) followed by further annealing after the 800 °C

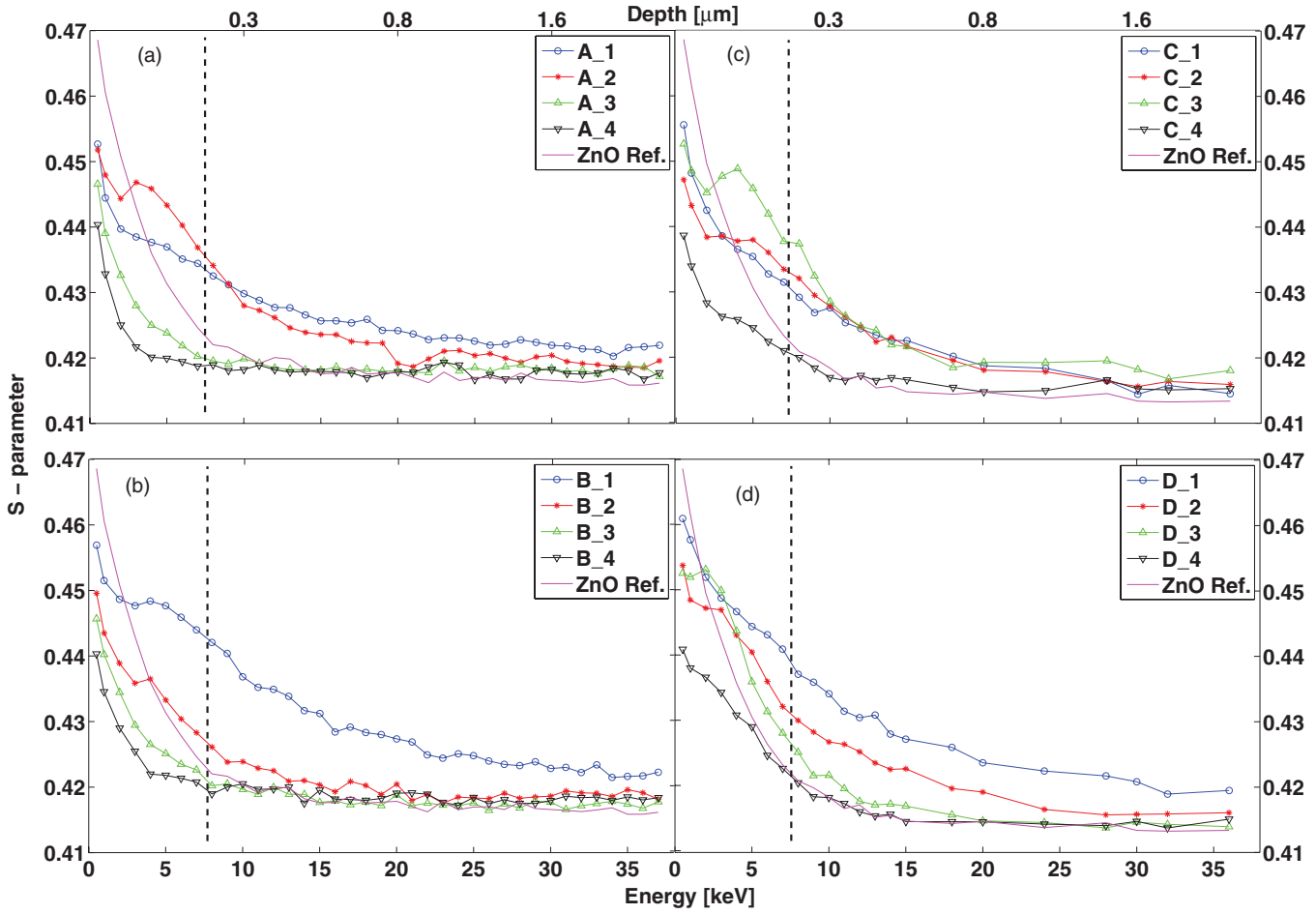

FIG. 2. (Color online) *S* parameter as a function of positron implantation energy/depth for wafers A–D plotted in panels (a)–(d), respectively. The dashed lines indicate the projected range of the Na implants.

and 950 °C treatment (B_3 and B_4, respectively). Here, it is worth noting that the redistribution of Na occuring in B_2 [see Fig. 1(b)] does not take place in A_2 [see Fig. 1(a)]. Consistent with the previous discussion, in *W*-*S* data for B_1, Fig. 3(b), yield a slope directed toward the HT-ZnO point while for B_2 the slope is shifted toward the ZnO-bulk point. For B_3, the data converge close to the ZnO-bulk point, indicating a low content of open-volume defects. Further increase of the temperature shifts the data (B_4) closer to the HT-ZnO point, in accordance with decreasing/increasing Na/Li concentrations, respectively [cf. Fig. 1(b)]. For B_3, the body of the data obey the V_{Zn} line and the V_{Zn} concentration is estimated[31] to be $\sim 7 \times 10^{15}$ cm^{-3}. The short positron diffusion length, indicated by the rapid decrease of the *S* parameter from surface to bulk value [e.g., A_4 and B_4 in Figs. 2(a) and 2(b)], suggests the presence of negatively charged ions with annihilation parameters similar to the ZnO lattice, possibly Na_{Zn}^{-}.

Qualitatively different behavior is observed in wafers C and D. Specifically, in wafer C, annealing at 600 (C_2) and 800 °C (C_3) leads to clustering of vacancies, mainly in the surface tail of the damage profile. The clusters are partly removed by the 950 °C anneal (C_4), but some defects still remain, evidenced by the change in the slope of the *S*-parameter curve after the first few data points from the surface [both in Figs. 2(c) and 2(d)].

In accordance with the fact that the preanneals at 1500 °C reduce the Li concentration to the 10^{15} cm^{-3} range, all the data slopes in Figs. 3(c) and 3(d) are directed toward the ZnO-bulk point and the V_{Zn} concentrations are estimated to be $\sim 1.4 \times 10^{16}$ and $\sim 7 \times 10^{15}$ cm^{-3} in samples C_4 and D_3, respectively. It should be noted that even if the difference between the samples C_4 and D_3 is small, it is statistically significant. A detailed examination of Figs. 3(c) and 3(d) unveils that the D_3 data are close to the ZnO reference point, while the C_4 data are clearly shifted toward the V_{Zn} point. The near surface defects responsible for the large deviation from the V_{Zn} line in Fig. 3(c) and 3(d), are attributed to the polishing process,[25] and the similarity between polishing- and implantation-induced defects has also been observed previously by other authors.[37] In contrast, for wafer D, the S parameter decreases monotonously at R_p with increasing temperature, Fig. 2(d), which is presumably to be associated with the increased presence of Na.

IV. DISCUSSION

A. Na configurations and its interplay with Li in ZnO

Park *et al.*[17] and Wardle *et al.*[18] have calculated the formation energies for interstitial and substitutional Li and Na (Li_i,

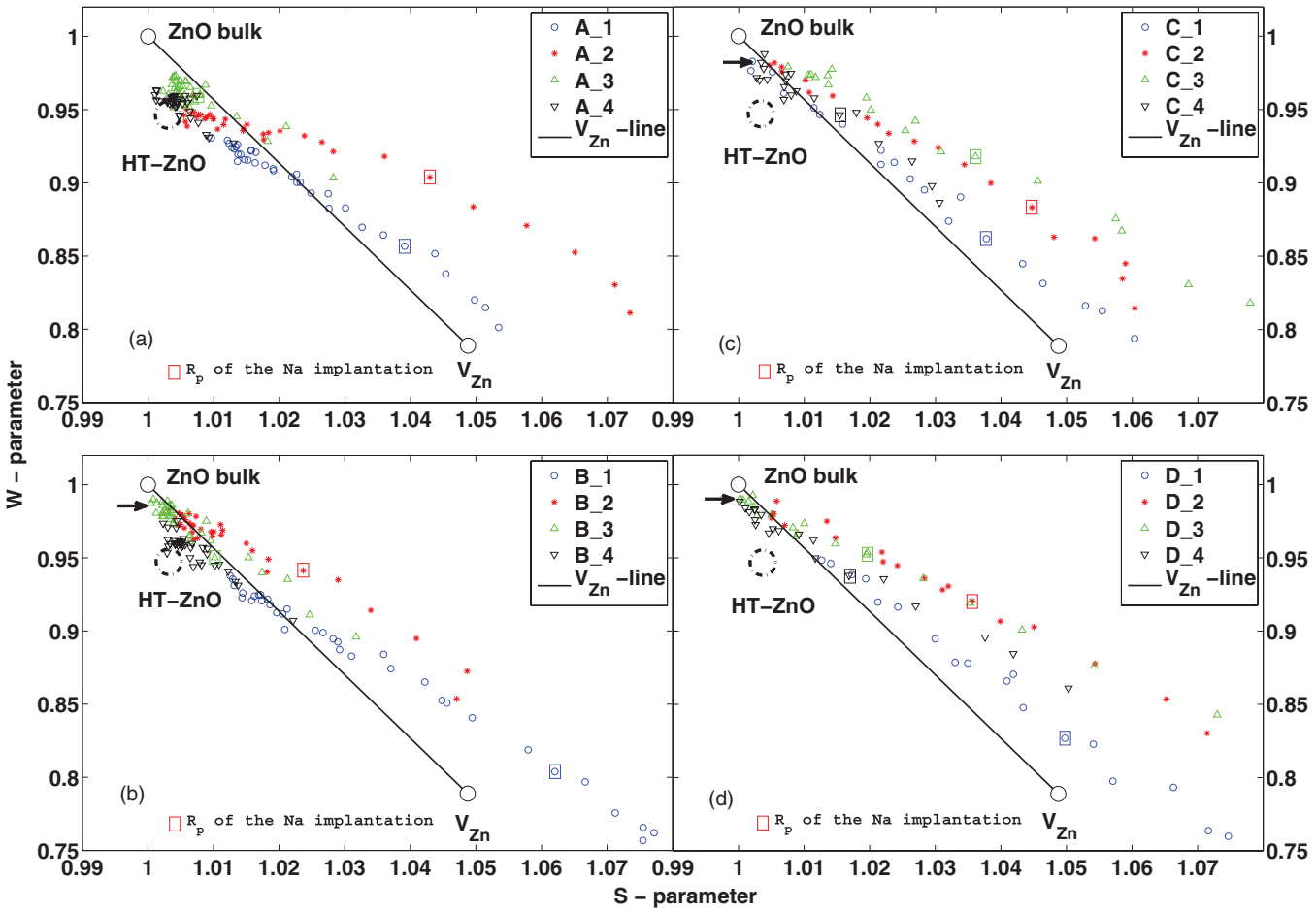

FIG. 3. (Color online) *W-S* plots for wafers A–D [(a)–(d) panels, respectively]. The arrows indicate the regions used to evaluate the V_{Zn} concentrations. The data points marked with squares correspond to a positron implantation energy of ∼8 keV, so that the mean penetration depth corresponds to the R_p. Surface related annihilation points have been omitted for clarity.

Li_{Zn}, and Na_i, Na_{Zn}, respectively) as a function of E_F. Their results show that the concentration of Li_{Zn} (Na_{Zn}) prevails over the concentration of Li_i (Na_i)—meaning the defect has a lower formation energy—when E_F is close to the conduction band edge, but Li_i (Na_i) becomes favorable when E_F moves toward the valence band edge. Formation energies (E_{form}) of interstitial and substitutional Li (Na) are intercepting around the middle of the band gap, resulting in a self-compensation and thus highly resistive, but still *n*-type, material. Wardle *et al.*[18] also predicted that Na would be more stable on a zinc site as compared to Li, which has been experimentally confirmed.[22] Since $E_{form}(Na_{Zn}) + E_{form}(Li_i) < E_{form}(Na_i) + E_{form}(Li_{Zn})$, Na_i causes Li_{Zn} to change the configuration to Li_i, which will diffuse and eventually get trapped in the sample bulk.

The same interplay between Na and Li as discussed in Ref. 22 can be seen in Figs. 1(a) and 1(b). Nevertheless, at higher temperatures ($\gtrsim$800°C), a significant amount of Li is observed in the Na enriched regions, indicating that not all the available trap sites are occupied by Na. This can be due to a high dissociation rate of the Na-trap complex or that the diffusion source of Na is exhausted. The Na plateau level exceeds the HT-Li level (which most likely represents the equilibrium concentration during sample growth) by a factor of ∼2 in wafers A and B. The difference between the bulk level of Li and plateau levels of Na in samples B_2 and B_3 can be attributed to a 50–60 meV difference between the formation energies of Li_{Zn} and Na_{Zn}, assuming equilibrium conditions and no other limiting factors such as the supply of Li and Na or changes in E_F.

The Li concentration in Figs. 1(c) and 1(d) (wafers C and D) is $\sim 10^{-2} \times$HT-Li, and the behavior of Na and Li are very different relative to those in Figs. 1(a) and 1(b). In the C and D samples, the Li redistribution resembles that when other elements than Na are implanted, and may be explained in terms of evolution of the implantation-induced damage.[24] Notably, no Na redistribution above the background level is observed but only a reduction in the peak concentration, indicating strong out-diffusion through the surface. If the concentration of Na incorporated beyond the implanted region would be determined by the Na_{Zn} formation energy, one would expect similar concentrations in diffusion tails for wafers C and D as for wafers A and B provided that the E_F position is the same. However, E_F is high in the bulk of wafers C and D due to the lower Li concentration remaining after preannealing at 1500 °C.[19] Hence the concentration of Na_i, assumed to be the mobile species, is highly suppressed in the bulk of wafers C and D and out-diffusion via the surface prevails. However, it

is likely that a low diffusion flux of Na_i toward the bulk still exists, as corroborated by the depletion of Li from the mid-10^{15} to the mid-10^{14} cm^{-3} range in depth interval ~0.5–1.5 μm for sample D_3, Fig. 1(d).

B. Evolution of open-volume defects after Na implantion

The effect of Na on the evolution of open-volume defects is illustrated by Figs. 2(a) and 2(b) (wafers A and B, respectively). For wafer A, the *S* parameter increases first and then decreases with increasing temperature, while for wafer B, the *S* parameter decreases monotonously with increasing temperature. Hence, in wafer A, vacancies form large clusters at 600 °C, which then dissociate at higher temperature. However, such clustering of the vacancies is not observed in wafer B, which contains a factor of ten higher concentration of Na. A comparison of Figs. 3(a) and 3(b) shows that the data from wafer B are close to the ZnO-bulk point, while the data from wafer A are close to the HT-ZnO point.[20] Altogether, these results provide strong evidence for a reduction in the open volume of defects due to the presence of Na and more specifically due to the substitution of Li_{Zn} by Na_{Zn} at temperatures $\geqslant$600 °C. It can be noted that even if the Li-related positron signal is clearly stronger in the A than in the B samples, sample B_4 seems to exhibit a noticeable Li signal. This may be due to the subtle balance between Na and Li concentrations in the region probed by the positrons: [Na]/[Li] ~ 20 in sample B_3, while it is only ~5 in sample B_4 ([Na]/[Li] ~ 1–5 in the A samples) (brackets denote concentration values).

The PAS data for wafers C and D, [Figs. 2(c)–2(d) and 3(c)–3(d)] corroborate the evidence of Li_{Zn} to Na_{Zn} substitution in spite of the presence of residual polishing-induced defects remaining in the vicinity of the surface. Indeed, the trend of the *S* parameter at depths around R_p in wafer C is the same as for wafer A—first an increase and then a decrease as a function of temperature—and wafer D [see Fig. 2(d)] is similar to wafer B—decreasing monotonously as a function of temperature. All the data in Figs. 3(c) and 3(d) are aligned with the ZnO-bulk point and fall on, or above, the V_{Zn} line fully consistent with the fact that the pretreatment at 1500 °C removes Li. In addition, in wafer D (high Na dose), the data converge closer to the ZnO-bulk point than in wafer C, showing smaller concentration of open-volume defects.

For wafer A, the V_{Zn} concentration cannot be deduced from the PAS data because of the strong contribution from Li_{Zn}.[20,31] However, the data from wafers B (B_3), C (C_4), and D (D_3) can be used and the corresponding V_{Zn} contents are 7×10^{15}, 1.4×10^{16}, and 7×10^{15} cm^{-3}, respectively, where the influence by negatively charged impurities is neglected, as discussed previously.[34] Assuming that equilibrium conditions apply during the annealing and that the V_{Zn}'s are stable during cooling down, the following formation energies of V_{Zn} are obtained in these three samples: 1.44, 1.57, and 1.44 eV, respectively. According to theoretical estimates,[9] these values imply that the samples are somewhat Zn rich.

C. Migration and trapping of Na

For wafers A and B [see Figs. 1(a) and 1(b)], Na migrates during the post implantation annealing with a clear diffusion tail already at 600 °C for wafer B (B_2) but not for wafer A (A_2). This is in accordance with a higher absolute amount of Na on lightly bound sites immediately after the implantation for wafer B, due to the higher Na dose, suggesting Na_i's to be the diffusing species. The diffusion profiles for wafer B show characteristic TLD exhibiting a plateau level in the range of ~ 2–5 $\times$ 10^{17} Na/cm^3, which decreases with increasing temperature. Also in wafer A, the plateau level as well as the implantation peak decrease rapidly, and sample A_4 displays a profile resembling a solution of Fick's equation, equivalent to a dissociation-dominated TLD process. For all the samples displaying Na diffusion, the previously discussed interplay between Li and Na occurs in the Na-rich regions, corroborating that Li and Na compete for the same traps.

In wafers C and D [see Figs. 1(c) and 1(d)], the most striking feature is the absence of redistribution of the implanted Na, demonstrating the pronounced effect of the preannealing at 1500 °C on the migration process of Na. The preannealing decreases the Li concentration [as well as increases the Na concentration but in negligible amount compared with the Na contents in the diffusion tails in Figs. 1(a) and 1(b)], and there are at least three possible scenarios for the evolution of the TLD process of Na: (i) the nature of the traps is the same for Li and Na, and they are strongly reduced in concentration during the pretreatment, (ii) Li_{Zn} is the trap for the diffusing Na, and/or (iii) the Na flux is greatly reduced by the pretreatment (see discussion in Sec. IV A).

The strong interplay between Li and Na, and the reduction in concentration of open-volume defects in Na-rich regions show that Li_{Zn} is, indeed, a trap for the diffusing Na species. This can occur via, for instance, the reaction $Na_i^+ + Li_{Zn}^- \rightarrow Na_{Zn}^- + Li_i^+$ in which the released Li_i's are highly mobile and subsequently would be trapped in the bulk through the reaction $Li_i^+ + V_{Zn}^{2-} \rightarrow Li_{Zn}^-$ (other reactions are also possible, including pair formation $Li_i - Li_{Zn}$).[18] However, this can not explain why the Na concentration exceeds the HT-Li level in samples A_3 and B_2–B_4, so an additional process must take place. Under equilibrium conditions, V_{Zn} is maintained and in *n*-type samples, the Na concentration is to a large extent anticipated to be controlled by the formation energy of Na_{Zn}; as discussed in Sec. IV A, a value lower by only ~50 meV than that of Li_{Zn} accounts for the difference between the HT-Li level and the Na plateau level in the samples A_3 and B_2–B_4. Thus the reaction $Na_i^+ + V_{Zn}^{2-} \rightarrow Na_{Zn}^-$ is regarded as highly plausible.

V. CONCLUSIONS

In conclusion, SIMS and PAS have been applied to study impurity migration and evolution of open-volume defects in Na^+ implanted HT-ZnO samples. In contrast to most other elements, the presence of Na decreases the concentration of open-volume defects upon post-implant annealing and at temperatures exceeding 600 °C, Na redistributes in a trap-limited diffusion mode correlating with the concentration of Li. A dominating trap for the migrating Na atoms is substitutional Li (Li_{Zn}), most likely via the reaction $Na_i^+ + Li_{Zn}^- \rightarrow Na_{Zn}^- + Li_i^+$, as supported by theoretical estimates of formation energies. However, this process is not sufficient to explain all the experimental observations and zinc vacancies

are also believed to contribute to the Na trapping via the $Na_i^+ + V_{Zn}^{2-} \rightarrow Na_{Zn}^-$ reaction; assuming the formation energy of Na_{Zn} to be ∼50 meV lower than that of Li_{Zn}, this reaction accounts for the fact that the Na concentration can exceed the bulk (equilibrium) Li concentration by about a factor of two.

ACKNOWLEDGMENTS

The authors gratefully acknowledge the financial support from the Norwegian Research Council through the NANOMAT, FRIENERGI, and FRINAT programs, the Academy of Finland, and NordForsk.

*p.t.neuvonen@smn.uio.no

[1] D. G. Thomas, J. Phys. Chem. Solids **15**, 86 (1960).

[2] Y. R. Ryu, T. S. Lee, J. A. Lubguba, H. W. White, Y. S. Park, and C. J. Youn, Appl. Phys. Lett. **87**, 153504 (2005).

[3] A. Tsukazaki, M. Kubota, A. Ohtomo, T. Onuma, K. Ohtani, H. Ohno, S. F. Chichibu, and M. Kawasaki, Jpn. J. Appl. Phys. **44**, L643 (2005).

[4] D. C. Reynolds, C. W. Litton, D. C. Look, J. E. Hoelscher, B. Claflin, T. C. Collins, J. Nause, and B. Nemeth, J. Appl. Phys. **95**, 4802 (2004).

[5] K. Maeda, M. Sato, I. Niikura, and T. Fukuda, Semicond. Sci. Technol. **20**, S49 (2005).

[6] S. E. Harrison, Phys. Rev. **93**, 52 (1954).

[7] A. R. Hutson, Phys. Rev. **108**, 222 (1957).

[8] A. F. Kohan, G. Ceder, D. Morgan, and C. G. Van de Walle, Phys. Rev. B **61**, 15019 (2000).

[9] A. Janotti and C. G. van de Walle, Phys. Rev. B **76**, 165202 (2007).

[10] A. Janotti and C. G. van de Walle, Appl. Phys. Lett. **87**, 122102 (2005).

[11] R. Schifano, E. V. Monakhov, L. Vines, B. G. Svensson, W. Mtangi, and F. D. Auret, J. Appl. Phys. **106**, 043706 (2009).

[12] E. V. Monakhov, A. Yu. Kuznetsov, and B. G. Svensson, J. Phys. D **42**, 153001 (2009).

[13] C. G. van de Walle, Phys. Rev. Lett. **85**, 1012 (2000).

[14] A. Janotti and C. G. van de Walle, Rep. Prog. Phys. **72**, 126501 (2009).

[15] S. B. Zhang, S.-H. Wei, and A. Zunger, J. Appl. Phys. **83**, 3192 (1998).

[16] S.-H. Wei and S. B. Zhang, Phys. Rev. B **66**, 155211 (2002).

[17] C. H. Park, S. B. Zhang, and S.-H. Wei, Phys. Rev. B **66**, 073202 (2002).

[18] M. G. Wardle, J. P. Goss, and P. R. Briddon, Phys. Rev. B **71**, 155205 (2005).

[19] B. G. Svensson, T. M. Børseth, K. M. Johansen, T. Maqsood, R. Schifano, U. Grossner, J. S. Christensen, L. Vines, P. Klason, Q. X. Zhao *et al.*, Mater. Res. Soc. Symp. Proc. **1035**, L04–01 (2008).

[20] K. M. Johansen, A. Zubiaga, I. Makkonen, F. Tuomisto, P. T. Neuvonen, K. E. Knutsen, E. V. Monakhov, A. Yu. Kuznetsov, and B. G. Svensson, Phys. Rev. B **83**, 245208 (2011).

[21] K. Saarinen, P. Hautojärvi, and C. Corbel, *Identification of Defects in Semiconductors* (Elsevier, 1998), Vol. 51. ISBN 0080-8784.

[22] P. T. Neuvonen, L. Vines, A. Yu. Kuznetsov, B. G. Svensson, X. L. Du, F. Tuomisto, and A. Hallén, Appl. Phys. Lett. **95**, 242111 (2009).

[23] Note that an apparent difference in Li background concentration between B_1 and B_2 and the rest of the A and B samples in Figs. 1(a) and 1(b) is because samples B_1 and B_2 were measured under different conditions causing some charge buildup affecting the calibration of Li-related signals. The actual background Li content is expected to be the same as in all B-type samples, more specifically in the range of $2–4 \times 10^{17}$ cm^{-3}. However, no normalization was made because it did not affect the interpretations.

[24] T. Moe Børseth, F. Tuomisto, J. S. Christensen, E. V. Monakhov, B. G. Svensson, and A. Yu. Kuznetsov, Phys. Rev. B **77**, 045204 (2008).

[25] F. A. Selim, M. H. Weber, D. Solodovnikov, and K. G. Lynn, Phys. Rev. Lett. **99**, 085502 (2007).

[26] Z. Q. Chen, T. Sekiguchi, X. L. Yuan, M. Maekawa, and A. Kawasuso, J. Phys. Condens. Matter **16**, S293 (2004).

[27] Z. Q. Chen, M. Maekawa, S. Yamamoto, A. Kawasuso, X. L. Yuan, T. Sekiguchi, R. Suzuki, and T. Ohdaira, Phys. Rev. B **69**, 035210 (2004).

[28] Z. Q. Chen, M. Maekawa, A. Kawasuso, R. Suzuki, and T. Ohdaira, Appl. Phys. Lett. **87**, 091910 (2005).

[29] Z. Q. Chen, M. Maekawa, A. Kawasuso, S. Sakai, and H. Naramoto, J. Appl. Phys. **99**, 093507 (2006).

[30] Z. Q. Chen, M. Maekawa, A. Kawasuso, and H. Naramoto, Phys. Status Solidi C **4**, 3646 (2007).

[31] F. Tuomisto, V. Ranki, K. Saarinen, and D. C. Look, Phys. Rev. Lett. **91**, 205502 (2003).

[32] F. Tuomisto, K. Saarinen, D. C. Look, and G. C. Farlow, Phys. Rev. B **72**, 085206 (2005).

[33] A. Zubiaga, F. Tuomisto, V. A. Coleman, H. H. Tan, C. Jagadish, K. Koike, S. Sasa, M. Inoue, and M. Yano, Phys. Rev. B **78**, 035125 (2008).

[34] The possible presence of negatively charged ions is not accounted for and causes an underestimation of the V_{Zn} concentration.[24]

[35] C. Rauch, I. Makkonen, and F. Tuomisto, Phys. Rev. B **84**, 125201 (2011).

[36] T. Moe Børseth, F. Tuomisto, J. S. Christensen, W. Skorupa, E. V. Monakhov, B. G. Svensson, and A. Yu. Kuznetsov, Phys. Rev. B **74**, 161202 (2006).

[37] M. H. Weber, F. A. Selim, D. Solodovnikov, and K. G. Lynn, Appl. Surf. Sci. **255**, 68 (2008).